Efficacy of DYRK1A inhibitors in novel models of Down syndrome acute lymphoblastic leukemia

Authors

Shannon L. Carey-Smith,[1,2*] Maryam H. Simad,[1*] Kunjal Panchal,[1,2] Carlos Aya-Bonilla,[1] Hannah Smolders,[1] Sang Lin,[1] Jesse D. Armitage,[1] Vivien T. Nguyen,[1] Kathryn Bentley,[1] Jette Ford,[1] Sajla Singh,[1] Joyce Oommen,[1] Anouchka P. Laurent,[3] Thomas Mercher,[3] John D. Crispino,[4] Andrew P. Montgomery,[5] Michael Kassiou,[5] Thierry Besson,[6] Emmanuel Deau,[7] Laurent Meijer,[7] Laurence C. Cheung,[1,2,8] Rishi S. Kotecha[1,2,9,10] and Sébastien Malinge[1,2,10]

[1]Telethon Kids Cancer Center, Telethon Kids Institute, Perth, Western Australia, Australia; [2]Curtin Medical School, Curtin University, Perth, Western Australia, Australia; [3]U1170 INSERM, Gustave Roussy, Villejuif, France; [4]Department of Hematology, St Jude Children's Hospital, Memphis, TN, USA; [5]School of Chemistry, University of Sydney, New South Wales, Australia; [6]University Rouen Normandie, INSA Rouen Normandie, CNRS, COBRA UMR 6014, Rouen, France; [7]Perha Pharmaceuticals, Perharidy Peninsula, Roscoff, France; [8]Curtin Health Innovation Research Institute, Curtin University, Perth, Western Australia, Australia; [9]Department of Clinical Hematology, Oncology, Blood and Marrow Transplantation, Perth Children's Hospital, Perth, Western Australia, Australia and [10]University of Western Australia, Perth, Western Australia, Australia

**SLC-S and MHS contributed equally as first authors.*

Correspondence:
S. MALINGE - sebastien.malinge@telethonkids.org.au

https://doi.org/10.3324/haematol.2023.284271

Efficacy of DYRK1A inhibitors in novel models of Down syndrome acute lymphoblastic leukemia

Shannon L. Carey-Smith[1,2,*], Maryam H. Simad[1*], Kunjal Panchal[1,2], Carlos Aya-Bonilla[1], Hannah Smolders[1], Sang Lin[1], Jesse D. Armitage[1], Vivien T. Nguyen[1], Kathryn Bentley[1], Jette Ford[1], Sajla Singh[1], Joyce Oommen[1], Anouchka P. Laurent[3], Thomas Mercher[3], John D. Crispino[4], Andrew P. Montgomery[5], Michael Kassiou[5], Thierry Besson[6], Emmanuel Deau[7], Laurent Meijer[7], Laurence C. Cheung[1,2,8], Rishi S. Kotecha[1,2,9,10] and Sébastien Malinge[1,2,10]

[1]Telethon Kids Cancer Centre, Telethon Kids Institute, Perth, WA, Australia

[2]Curtin Medical School, Curtin University, Perth, WA, Australia

[3]U1170 INSERM, Gustave Roussy, Villejuif, France

[4]Department of Hematology, St Jude Children`s Hospital, Memphis, TN, USA

[5]School of Chemistry, University of Sydney, NSW, Australia

[6]University Rouen Normandie, INSA Rouen Normandie, CNRS, COBRA UMR 6014, 76000 Rouen, France

[7]Perha Pharmaceuticals, Perharidy Peninsula, Roscoff, France

[8]Curtin Health Innovation Research Institute, Curtin University, Perth, WA, Australia

[9]Department of Clinical Haematology, Oncology, Blood and Marrow Transplantation, Perth Children's Hospital, Perth, WA, Australia

[10]University of Western Australia, Perth, WA, Australia

*SLCS and MHS contributed equally to the study

Supplementary Figures and legends

Supplementary Figure 1

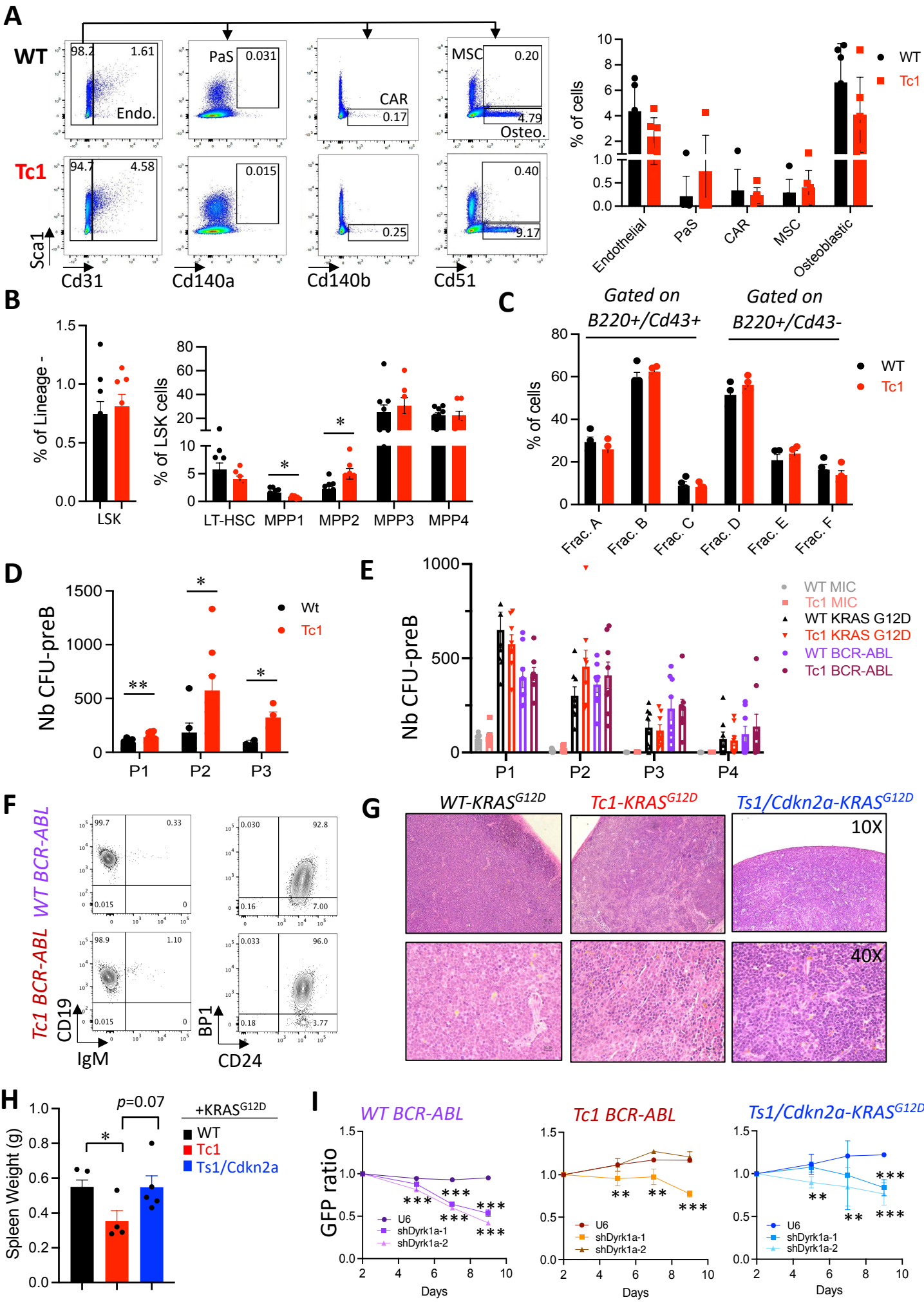

Supplementary Figure 1: Establishment of murine DS-ALL cells.

A. Representative flow plots comparing the bone marrow stroma of 8-10 week old wild-type (WT) and trisomic (Tc1) mice, gated on CD45-Ter119- and depicting the percentage of endothelial cells (endo, CD31-positive), CD31-negative PaS (PDGFRa(Cd140a)+/Sca1+), Cxcl12-abundant reticular cells (CAR, PDGFRb(cd140b)+/Sca1-), mesenchymal stem cells (MSC, Sca1+/CD51+) and osteoblastic cells (osteo, Sca1-/CD51+). *Right panel*: box plot integrating all data (n=6). **B.** Bar graph displaying the percentage of the different hematopoietic stem cells and progenitors in 8-10 week old mice (n=7-9); *p<0.05. LSK = Lineage-negative/Sca1+/Kit+, LT-HSC (Long-term hematopoietic stem cells, LSK+CD34-FLT3-CD150+CD48-), MPP1 (multipotent progenitor 1, LSK+CD34+FLT3-CD150+CD48-), MPP2 (LSK+CD34+FLT3-CD150+CD48+), MPP3 (LSK+CD34+FLT3-CD150-CD48+), MPP4 (LSK+CD34+FLT3+CD150-CD48+). **C.** Bar graph displaying the proportion of the hardy fraction in the bone marrow of WT and Tc1 mice (n=4); Fraction A (B220+CD43+CD24-BP1-), Fraction B (B220+CD43+CD24+BP1-), Fraction C (B220+CD43+CD24+BP1+), Fraction D (B220+CD43-IgM-IgD-), Fraction E (B220+CD43-IgM+IgD-) and Fraction F (B220+CD43-IgM+IgD+). **D.** Number of colony-forming unit (CFU)-preB colonies obtained from 8-10 week old WT and Tc1 donor bone marrow cells over 3 passages (n=8-9); *p<0.05, **p<0.01. **E.** Number of CFU-preB colonies obtained from sorted mCherry-positive bone marrow progenitor cells transduced with $KRAS^{G12D}$, BCR-ABL retroviruses compared to empty vector retroviruses (MIC = MSCV-IRES-mCherry), over 4 passages (n=8). **F.** Phenotype of the WT-BCR-ABL and Tc1-BCR-ABL cell lines assessing surface expression of CD19, IgM, BP1 and CD24. **G.** Representative spleen sections from WT-$KRAS^{G12D}$, Tc1-$KRAS^{G12D}$ and Ts1/cdkn2a-$KRAS^{G12D}$ primary recipients, stained with hematoxylin and eosin (10X and 40X magnification). **H.** Average spleen weight at endpoint in WT-$KRAS^{G12D}$ (n=5), Tc1-$KRAS^{G12D}$ (n=4) and Ts1/Cdkn2a-$KRAS^{G12D}$ (n=5) irradiated recipient mice; *p<0.05. **I.** Ratio of GFP-expressing Banshee vectors encoding two shDyrk1a compared to empty Banshee-U6 counterparts over 9 days in the murine WT-BCR-ABL, Tc1-BCR-ABL and Ts1/cdkn2a-$KRAS^{G12D}$ cells (n=4 replicates); **p<0.01, ***p<0.001.

Supplementary Figure 2

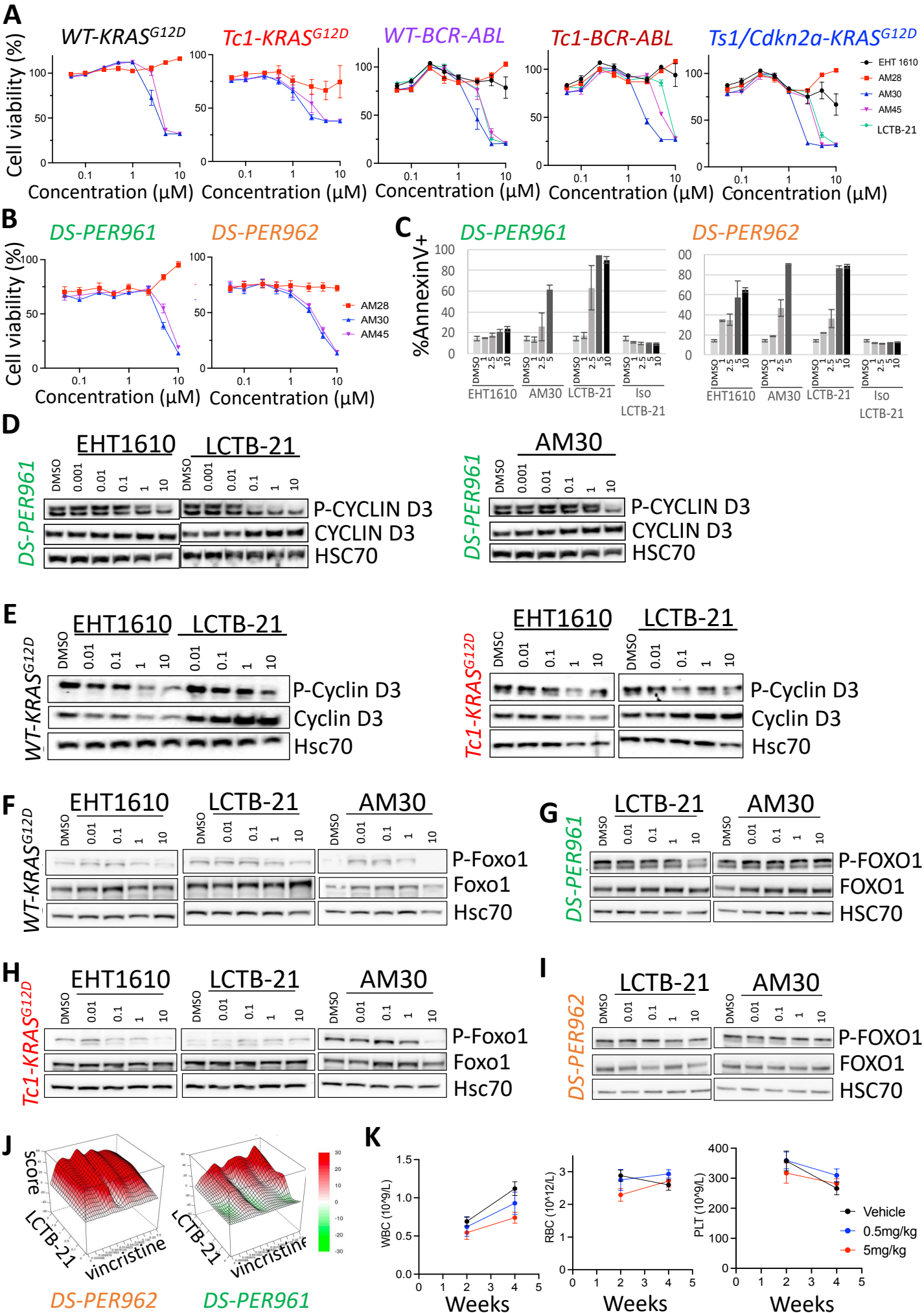

Supplementary Figure 2: Preclinical testing of new DYRK1A inhibitors in non-DS and DS-ALL.

A. Dose-response curves for EHT1610, Leucettinib-21 (LCTB-21), AM28, AM30 and AM45 in murine cell lines. **B.** Dose-response curves for AM28, AM30 and AM45 in human DS-PER961 and DS-PER962 cell lines. **C.** Bar graphs showing the impact of increasing doses 1µM, 2.5µM, 5µM and 10µM of the DYRK1A inhibitors EHT1610, AM30, LCTB-21 and its inactive isomer iso-Leucettinib-21 (Iso LCTB-21) on cell viability of DS-PER961 and DS-PER962 at 48 hours assessed by flow cytometry (AnnexinV-positive cells). **D.** Western blots of phospho-Cyclin D3 performed from protein extracted from the DS-PER961 human cell line after a 6 hour treatment with increasing doses (in µM) of the DYRK1A inhibitors EHT1610, Leucettinib-21 and AM30, compared to treatment with DMSO. **E.** Western blots of phospho-Cyclin D3 performed from protein extracted from WT-KRAS^{G12D} and Tc1-KRAS^{G12D} murine cells after a 6 hour treatment with increasing doses (in µM) of the DYRK1A inhibitors EHT1610 and Leucettinib-21, compared to treatment with DMSO. **F-I.** Assessment of FOXO1 (Ser326) phosphorylation in response to DYRK1A inhibition (6 hour treatment) in (**F**) murine WT-KRAS^{G12D}, (**G**) human DS-PER961 (KRAS^{G12S}), (**H**) murine Tc1-KRAS^{G12D} and (**I**) human DS-PER962 (CRLF2-rearranged/JAK2^{I682F}) cells. **J.** Representative plots showing synergy between LCTB-21 and vincristine in DS-PER962 and DS-PER961 cell lines. **K.** Blood count assessment showing WBC (white blood cell count), RBC (red blood cell count) and PLT (platelet counts) at week 2 and week 4 of treatment with 0.5 mg/kg and 5 mg/kg of Leucettinib-21 compared to vehicle in the DS06 patient-derived xenograft (n=3 per group and per timepoint).

Supplementary Figure 3

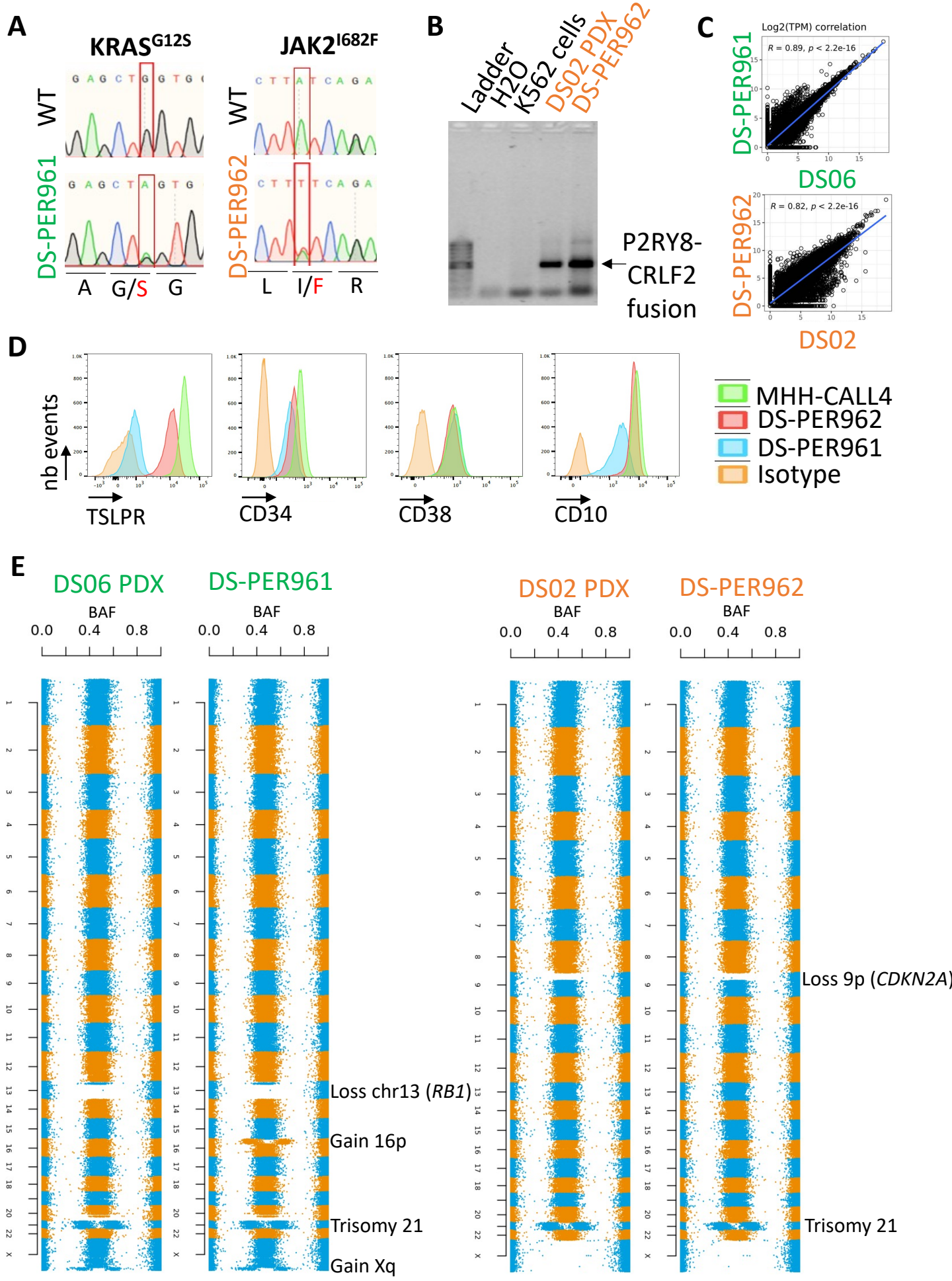

Supplementary Figure 3: Characterization of human DS-ALL cell lines.

A. Sanger sequencing of genomic DNA confirming the presence of the *KRAS*^{G12S} and *JAK2*^{I682F} mutations found in the DS-PER961 and DS-PER962 cell lines respectively. **B.** Validation of the P2RY8-CRLF2 fusion transcript in the DS02 patient-derived xenograft (PDX) and DS-PER962 cell line compared to K562 control cells (primer sequences are indicated in supplemental table 2). **C.** Spearman correlation of the transcriptional profiles obtained in the DS-PER961 and DS-PER962 cell lines (Y-axis) compared to the PDX model they originate from (X-axis). RNA sequencing files are available via the Gene Expression Omnibus (GEO) database under the accession number GSE245056. **D.** Representative flow plots comparing the Mean Fluorescence Intensity (MFI) for the surface markers TSLPR, CD34, CD38 and CD10 in the DS-PER961 (in blue) and DS-PER962 (in red) compared to MHH-CALL4 cells (in green); isotypes are represented in orange. **E.** Bi-allelic frequencies obtained from SNP arrays (HumanCytoSNP-12 BeadChip (HumanCytoSNP-12v2.1; Illumina) comparing DS-PER961 and DS-PER962 cell lines with the PDX they originate from, showing that the cell lines are relatively stable at the genomic level.